Assessment of load history effects on ductile initiation fracture toughness by the Gurson-Tvergaard-Needleman model

A.P. Jivkov[1,*], J.K. Sharples[1], P.J. Budden[2]
[1]*Serco, Risley, Warrington, UK;* [2]*British Energy, Barnwood, Gloucester, UK.*

Abstract

Residual stresses may reduce the apparent ductile fracture toughness of structural steels. However, prior load excursions may alleviate this reduction. Effects of several load histories on ductile fracture initiation are investigated using finite element analyses of compact tension specimens. The Gurson-Tvergaard-Needleman micromechanical model is used, where void volume fraction in the crack tip vicinity measures local damage. Analysis without load history, with three tensile residual stress levels, and three tensile overload levels after each residual stress are performed. Evolutions of several global and local parameters with local damage are presented. Ductile fracture initiation is assumed when local damage attains a critical value. The reduction of fracture toughness is shown to increase with increasing residual stress levels. Departure from this trend is observed for high residual stresses and is explained by damage-band formation. Increasing overloads are shown to increasingly mitigate the detrimental effects of residual stress.

1. Introduction

Classical fracture mechanics assessment involves global concepts, such as strain energy release rates, contour integrals or stress intensity factors which result from an overall energetic analysis of a cracked structure. Safety is assured when a global parameter is demonstrated to be less than a lower bound estimate from experimental fracture toughness tests of high constraint geometries. In many practical situations, e.g. low constraint geometries, the classical assessment may be rather conservative. This may also be the case when assessing cracks in residual stress fields subjected to load history, since the classical methods do not take into account the fact that the stresses may be reduced from those at start of life. Local approaches offer an alternative methodology for carrying out fracture mechanics assessments, intrinsically accounting for the real geometry and the history of loading [1]. This methodology requires a detailed finite element (FE) solution of the cracked geometry to acquire precise knowledge of the local stress and strain fields and a micro-mechanical model of the material's fracture behaviour in a fracture process zone surrounding the crack tip. Micro-mechanical models suitable for brittle and ductile fracture have been developed over the last

three decades (see references in [1]). Each of these models contains a number of material dependent parameters that must be properly defined to give meaningful predictions.

The work reported here is focused on ductile fracture and explores the possibility to predict load history effects using an appropriate local approach. An FE model of an enlarged compact tension specimen, C(T), described in Section 2, is used to assess the effect of residual stresses and possible subsequent tensile overloads on the load carrying capacity and fracture toughness. The material selected is 316 stainless steel weld metal. The micro-mechanical behaviour of this material is described by the Gurson-Tvergaard-Needleman (GTN) ductile damage model [2, 3]. This is the most widely used model from a class of pressure-dependent (porous-plasticity) material models, where the void volume fraction serves as a measure of damage. Typical parameters are selected from previous experience with this model applied to similar types of materials [4]. The void volume fraction at the first integration point ahead of the crack is accepted as a local damage parameter. Crack growth or ductile tearing is assumed to initiate when the local damage attains a prescribed critical value. The C(T) geometry without the crack is subjected to a number of loading histories designed to develop different initial, i.e. prior to crack introduction, stress and strain fields in the vicinity of the crack tip. The simulations are performed with ABAQUS [5], where the GTN model is implemented with a user-defined material procedure [3].

The results, presented in Section 3, illustrate the effects of the various load histories on the load carrying capacity of the specimen, as well as on the "global" and the "local" fracture toughness. These three parameters are defined as the load level, the "global" and the "local" crack driving forces at critical damage, respectively. Global crack driving forces, essentially far-field J-integrals, are calculated from the load versus load line displacement curves using the prescription of the ASTM E1820 fracture toughness testing standard [6] and illustrate the expected outcomes from an experimental programme. Local crack driving forces are defined as the near-field J-integrals. These are calculated as domain-independent integrals, the formulation of which accounts for the effects of any initial stresses and plastic strains [7]. For the cases with very high tensile residual stresses and no or very low tensile overloads, the results appear to be unreliable. This is explained by the formation of damage bands inclined with respect to the crack plane prior to attaining critical damage. Discussion and conclusions are given in Section 4.

2. Model description

The model geometry, half of the C(T) specimen due to symmetry, and the finite element mesh used are shown in Fig. 1, with the top figure showing the overall geometry with the positions of the boundary conditions applied, and the bottom figure showing the notch root detail and near crack tip region with a coordinate

system centred at the tip. Eight-node quadratic plane strain finite elements with reduced integration are used. The dimensions are selected in order to maintain approximate small scale yielding conditions for crack driving forces up to the expected material fracture toughness. The wide notch geometry is selected in order to introduce appropriate residual stress fields by application of an initial, compressive load. The nodes, depicted as crack flank in the bottom figure, have the same boundary conditions as the ligament prior to crack introduction, as described in the load history cases below.

In ductile metals, such as the 316 stainless steel considered here, fracture is a multi-step process in which a number of micro-mechanical mechanisms occur concurrently: (i) micro-voids are nucleated by de-cohesion of second-phase inclusions, (ii) micro-voids grow due to plastic straining, (iii) localised diffuse necking occurs as micro-void coalescence begins, and (iv) fracture occurs caused by coalescence of micro-voids and the tearing of the ligaments between them. The GTN model [2, 3] is a pressure-dependent plasticity constitutive model that aims to account for the nucleation, growth and coalescence of micro-voids and the mechanisms of ductile rupture via evolution of damage.
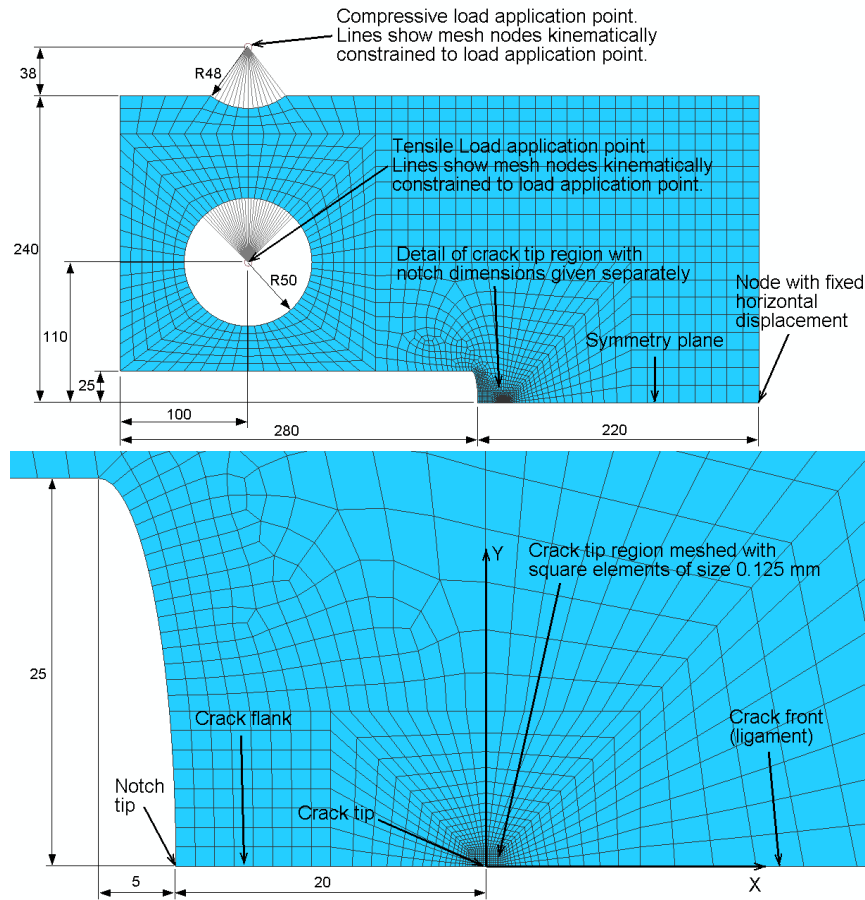
Figure 1. Geometry of compact tension specimen and finite element mesh used. All dimensions are in millimetres.

3

The material response is described with a hypothetical separation between the behaviour of a fully dense matrix, i.e. material without any voids, and the behaviour of the voids. This is achieved by the introduction of two continuous internal state variables - the equivalent plastic strain of the fully dense matrix $\varepsilon^p_{eq(M)}$, and void volume fraction f, representing micro-voids distributed continuously throughout the matrix. The material behaviour is governed by the equivalent (von Mises) stress σ_{eq}, hydrostatic stress σ_m, equivalent plastic strain ε^p_{eq}, and volumetric plastic strain ε^p_m of the voided matrix, as well as the evolution of the flow stress σ_0 with $\varepsilon^p_{eq(M)}$ of the fully dense matrix. Note that ε^p_m is not necessarily zero as in classical pressure-independent plasticity. The yield function Φ is isotropic and identical to the plastic potential g, given by [3]

$$\Phi = g = \left(\frac{\sigma_{eq}}{\sigma_0}\right)^2 + 2q_1 f^* \cosh\left(\frac{3q_2\sigma_m}{2\sigma_0}\right) - \left(1 + q_3 f^{*2}\right) = 0, \tag{1}$$

where q_1, q_2, q_3 are material constants and f^* is a modified void volume fraction described shortly. Data from uniaxial tensile tests of 316 stainless steel weld metal at room temperature are used to prescribe the material elastic behaviour with Young's modulus $E = 171$ GPa, Poisson's ratio $\nu = 0.294$, and evolution of σ_0 with $\varepsilon^p_{eq(M)}$ as isotropic hardening in a tabular form. The precise hardening behaviour used is given elsewhere [8]. The initial flow stress, used as a normalising parameter in some results presentation, is $\sigma_0 = 425$ MPa. The evolution of $\varepsilon^p_{eq(M)}$ is given by [3]

$$\dot{\varepsilon}^p_{eq(M)} = \frac{\sigma_{eq}\dot{\varepsilon}^p_{eq} + 3\sigma_m\dot{\varepsilon}^p_m}{(1-f)\sigma_0}, \tag{2}$$

where the dots represent rates of change of the corresponding variables. The initial condition for this internal variable is $\varepsilon^p_{eq(M)} = 0$. The evolution of f is given by [3]

$$\dot{f} = \frac{f_N}{S_N\sqrt{2\pi}}\exp\left[-\frac{1}{2}\left(\frac{\varepsilon^p_{eq(M)} - \varepsilon_N}{S_N}\right)^2\right]\dot{\varepsilon}^p_{eq(M)} + 3(1-f)\dot{\varepsilon}^p_m, \tag{3}$$

where the first term models the nucleation of new micro-voids, i.e. mechanism (i), and the second term models the growth of existing micro-voids, i.e. mechanism (ii). In the first term, ε_N and S_N are the mean and standard deviation of the nucleation strain assumed to obey a normal distribution, and f_N is the volume fraction of void nucleating particles. The initial condition for this internal variable is $f = f_0$, where f_0 is a material parameter, the initial void volume fraction. The coalescence of micro-voids, i.e. mechanism (iii), is modelled via an accelerated softening of the yield surface Eq. (1) introduced with f^*. This equals f up to a critical void volume fraction f_c, after which it increases more rapidly to

4

give increased softening as the micro-voids coalesce. Mechanism (iv) occurs at another level, denoted by f_f, when the local load carrying capacity is reduced to zero. This behaviour is represented by the relation [9]

$$f^* = \begin{cases} f, & f \leq f_c \\ f_c + \left(\dfrac{f_u^* - f_c}{f_f - f_c} \right)(f - f_c), & f_c < f < f_f \\ f_u^*, & f \geq f_f \end{cases} \tag{4}$$

where f_u^* is the value of f^* at zero stress, i.e. when f reaches f_f. The model parameters, selected from previous experience, are given in Table 1. The fracture process zone is assumed to be confined to the first element ahead of the crack tip of size 125 microns, where local damage is characterised by f evaluated at the integration point closest to the crack tip. The local damage is denoted by d to distinguish it from the field variable f. Initiation of ductile tearing is assumed to occur when d reached a critical value of $d_c = 0.15$.

Table 1. Parameters of the GTN model

f_0	f_c	f_f	f_u^*	f_N	ε_N	S_N	q_1	q_2	$q_3 = q_1^2$
0.00072	0.15	0.60	2/3	0.01	0.3	0.1	1.5	1.0	2.25

The FE model is subjected to 13 loading histories representing three levels of residual stresses, three levels of tensile overloads after each of the residual stress applications and a case of no load history prior to primary load. In the last case, denoted by V, primary load is applied to the cracked geometry of Fig. 1 via a prescribed displacement of the tensile load application point increasing from 0 to 2 mm. In all other cases, a case-specific load history is applied to the un-cracked geometry, which is then followed by an instantaneous crack introduction to the designed crack size of Fig. 1 and a primary load applied via 2 mm increase of the displacement of the tensile load application point relative to the position of the point after crack introduction. Illustration of the specific load histories for all cases except V is given in Fig. 2. The three residual stress cases, shown in the top left graph as R1, R2, R3, correspond to three magnitudes of applied compressive displacement, 3, 5, 10 mm, respectively. The three tensile overloads, denoted by O1, O2, O3, correspond to three magnitudes of applied tensile displacement, 0.5, 1.0, 1.5 mm, respectively. When applied after residual stress cases R1, R2, R3, these provide the notations used in the top right, bottom left, and bottom right graphs, respectively. Load line displacements and resulting reactions (loads) are monitored and recorded for the entire simulation duration for each load history case. Load-displacement histories during primary load step are used to calculate a global crack driving force, J, based on [6]. Loads and global crack driving forces are related to d, providing the load carrying capacity and the global fracture toughness, respectively, at d_c. The local crack driving force calculated as a near-field J-integral is also related to d, providing the local fracture toughness at d_c.
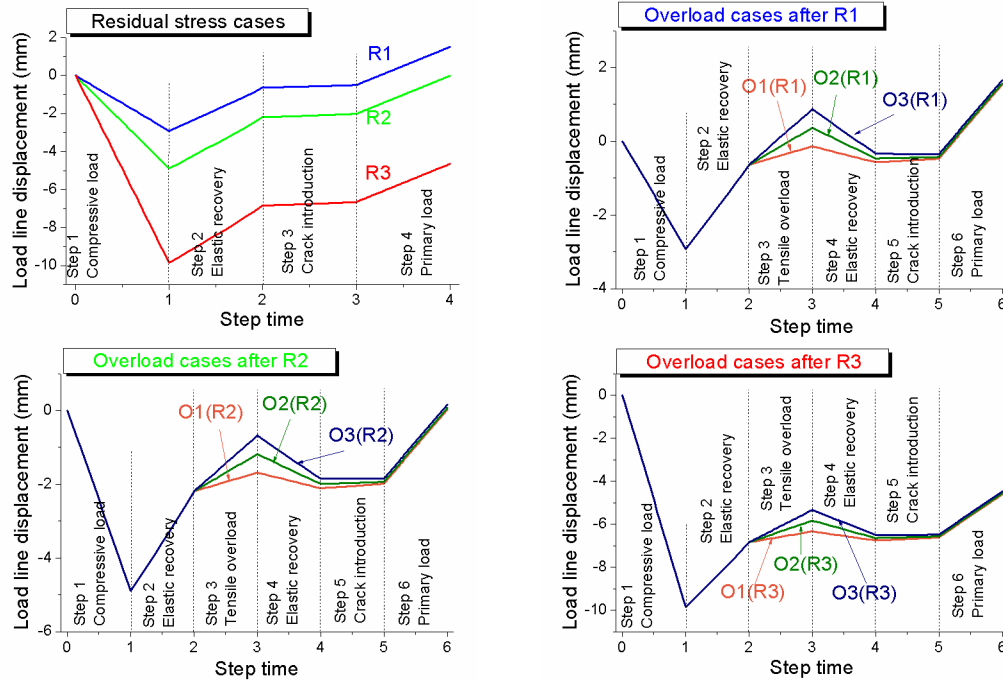
Figure 2. Loading histories applied to the FE model.

To allow for initial plastic strains, resulting from the load histories, an extended expression for calculating the *J*-integral developed in terms of equivalent domain integral and coded into a post-processing programme JEDI [7] is used.

3. Results

The load histories applied to the un-cracked specimen resulted in different stress and strain fields in the region where the crack was introduced prior to primary loading. The profiles of the stress normal to the crack (symmetry) plane before the crack introduction are shown in Fig. 3. The stresses and distances are normalized with $\sigma_0 = 425$ MPa, W = 400 mm. The top left graph shows the stress profiles resulting from the residual stress introduction process, i.e. end of Step 2 in Fig. 2. The other three graphs show the stress profiles resulting from the overloads application after each of the three residual stress levels, i.e. end of Step 4 in the corresponding three graphs in Fig. 2. The residual stress cases without overloads are also shown for comparison. Thus, these three graphs illustrate the state into which the crack is introduced for all cases apart from case V. The crack introduction is accompanied by a redistribution of stresses without any external loading. This redistribution yields changes in the plastic strain field in the crack tip vicinity causing changes in the local damage parameter. The developments of *d* are not shown here, but the local damage accumulated prior to primary loading will be exhibited as initial values in the following results. In all cases *d* at the end of crack introduction is less than d_c hence the initiation of crack growth (ductile tearing) is determined during the primary load step for all load history cases.
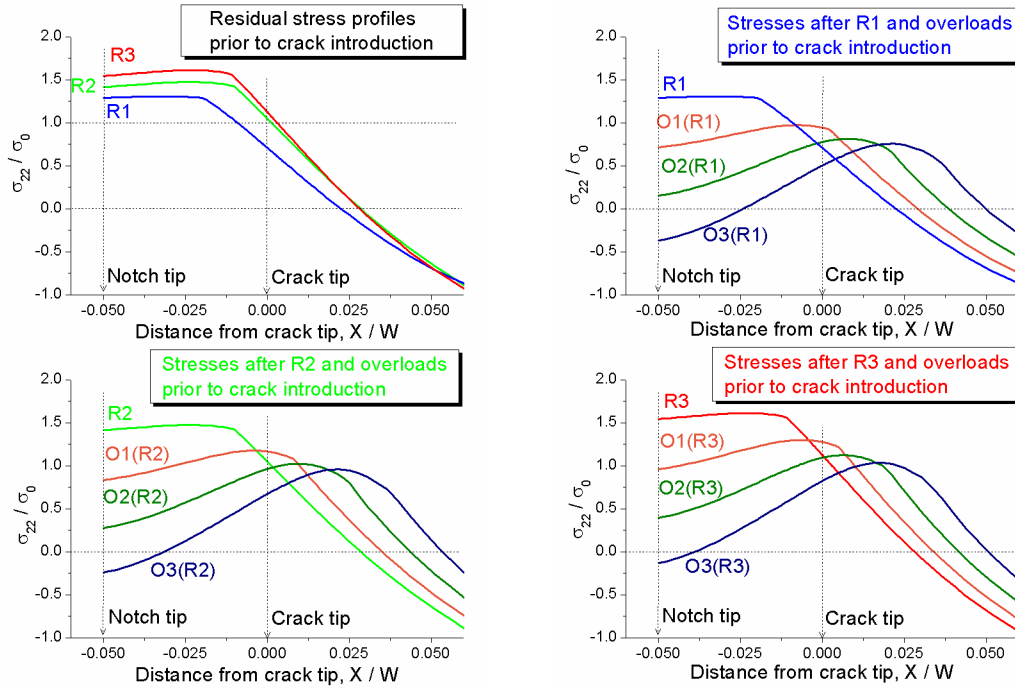
6

Figure 3. Stress profiles resulting from loadings of un-cracked specimen.

The development of the load with the local damage parameter, *d*, is shown in Fig. 4 and explained by the notations there. The reference case V is included in all three graphs for comparison. The numbers depicted in the graphs represent the predicted load carrying capacity for the corresponding experiment.
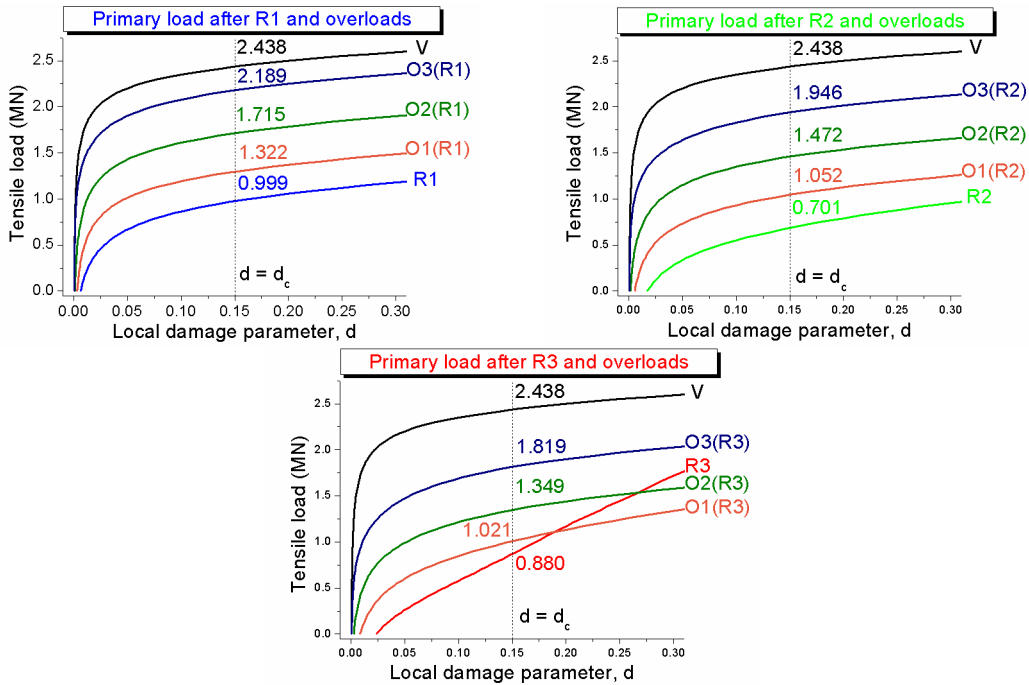

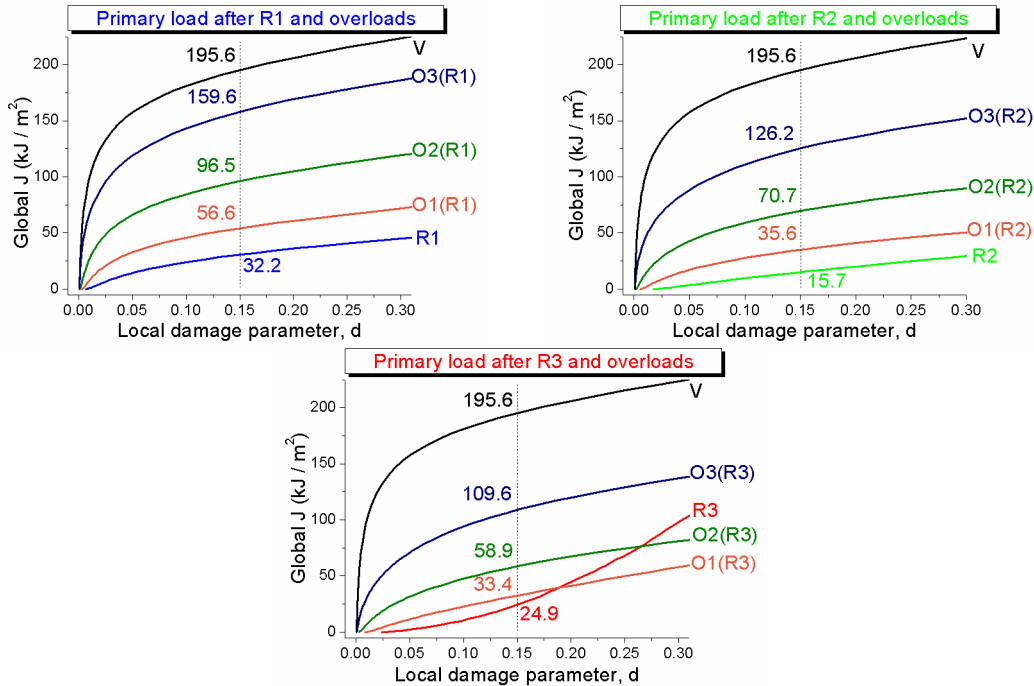Figure 4. Primary load vs local damage (Load carrying capacity marked).

Figure 5. Global *J* vs local damage (Global fracture toughness marked).

Similarly, the global *J* calculated from the load-displacement curves (not presented here) are shown in Fig. 5 as functions of *d*. The numbers depicted in the graphs represent the ductile initiation toughness predicted for experimental outcomes. The development of the corresponding near-field *J*-integrals with *d* are shown in Fig. 6, with the numbers depicting local fracture toughness.
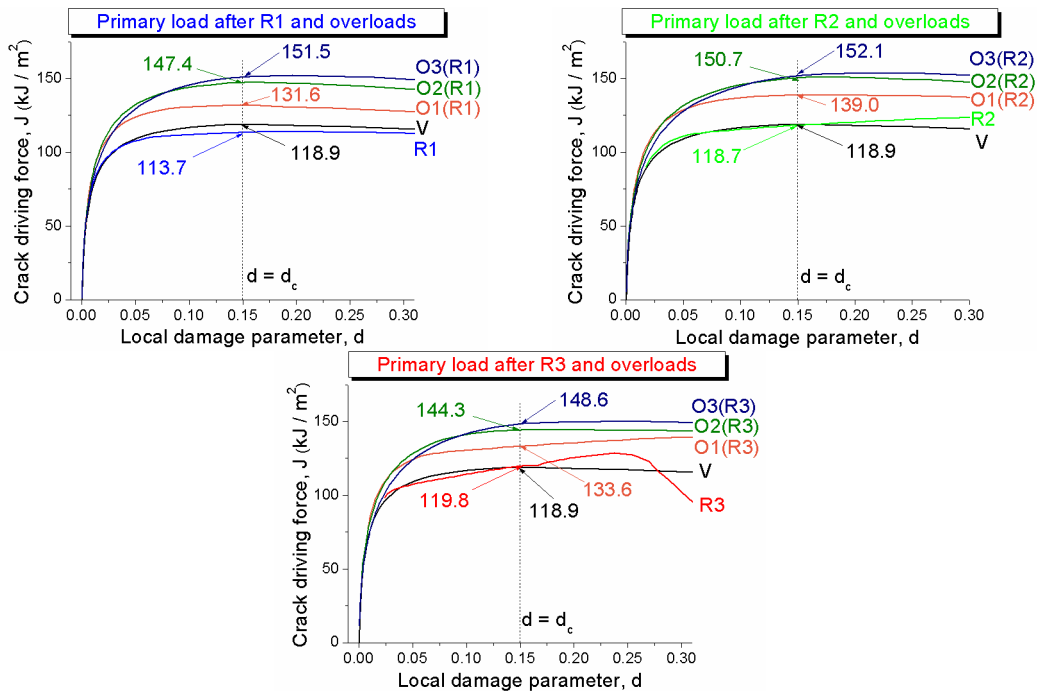

Figure 6. Near-field *J* vs local damage (Local fracture toughness depicted).

4. Discussion and conclusions

The results presented in Figs. 4 and 5 lead to the following conclusions. Tensile residual stresses in the crack tip vicinity have a substantial detrimental effect on the global load carrying capacity and the global fracture toughness. Tensile overloads in a component with tensile residual stresses can partially mitigate the detrimental effect of the residual stresses, increasing the global load carrying capacity and the global fracture toughness. The results presented in Fig. 6 show very little effect of the residual stresses on the local fracture toughness. Tensile overloads are predicted to increase the local fracture toughness relative to the underlying residual stress case, suggesting a dual beneficial effect of the overloads. However, the predicted local toughness values are higher than the toughness of the virgin material. Compared to the global behaviour this implies that for such load histories the use of the near-field *J*-integral as a fracture initiation criterion requires further investigation.

Comparison of the results for R2 and R3 in Figs. 4 and 5 suggests that the material with higher tensile residual stresses R3 performs better than R2, both in terms of higher load carrying capacity and higher global fracture toughness. The expected trend is that an increased residual stress level should result in decreased critical values. The unrealistic outcome is an indication that the criterion for ductile tearing initiation and the related local damage parameter selected in this work cannot be used universally. Strain-localisation analysis [9] and maps of damage distribution in the near-tip region have been used for qualitative explanation of this behaviour. It was found that strain localisation, local to the first integration point ahead of the crack tip, was possible in all load history cases studied prior to attaining critical damage. In cases R3 and O1(R3) the strain localisation was found to develop into a shear (damage) band inclined with respect to crack plane, i.e. a "slant fracture" mode was observed. The formation of a shear band renders the subsequent results for these cases unreliable and calls for an extended criterion for ductile tearing initiation that incorporates the observed behaviour. For all other cases studied, strain localisation was found to be contained locally throughout the loading history, suggesting stable continuation of the simulations after strain localisation as well as after attaining critical damage. The initiation of ductile tearing in such cases could be considered as coinciding with attaining a critical level of damage, i.e. the approach taken in this work might be sufficient. Further work is required for developing an initiation criterion of universal applicability.

References

[1] A. Pineau, Development of the local approach to fracture over the past 25 years: theory and applications, Int J Fract 138 (1-4) (2006) 139-166.

[2] V. Tvergaard, A. Needleman, Analysis of cup-cone fracture in a round tensile bar, Acta Metall 32 (1) (1984) 157-169.

[3] D.W. Beardsmore, M.A. Wilkes, A. Shterenlikht, An implementation of the Gurson-Tvergaard-Needleman plasticity model for Abaqus Standard using a trust region method, in: Proc. PVP2006-ICPVT-11 ASME Pres Vess Piping Div Conf, Vancouver, Canada, 2006, pp. 615-623.

[4] A.H. Sherry, M.A. Wilkes, Numerical simulation of tearing-fatigue interactions in 316L(N) austenitic stainless steel, Int J Pres Vess Piping 82 (12) (2005) 905-916.

[5] ABAQUS User's Manual, Dassault Systemes, 2007.

[6] ASTM E1820-08 Standard Test Method for Measurement of Fracture Toughness, ASTM, 2008.

[7] D.W. Beardsmore, A.H. Sherry, Allowance for residual stresses and material interfaces when calculating J in and close to welded joints, in: Proc. PVP2003 ASME Pres Vess Piping Conf, Cleveland, Ohio, USA, 2003, pp. 11-21.

[8] R.O. Howells, A.P. Jivkov, D.W. Beardsmore, J.K. Sharples, M.R. Goldthorpe, C.T. Watson, Local approach studies of the effect of load history on ductile fracture, in: Proc. PVP2008 ASME Pres Vess Piping Div Conf, Chicago, Illinois, USA, 2008.

[9] J. Besson, D. Steglich, W. Brocks, Modelling of plane strain ductile rupture, Int J Plasticity 19 (10) (2003) 1517-1541.